

Bulk ionization potentials and band alignments from three-dimensional periodic calculations as demonstrated on rocksalt oxides

Andrew J. Logsdail,^{1,*} David O. Scanlon,^{1,2} C. Richard A. Catlow,¹ and Alexey A. Sokol^{1,†}¹*University College London, Kathleen Lonsdale Materials Chemistry, Department of Chemistry, 20 Gordon St., London WC1H 0AJ, United Kingdom*²*Diamond Light Source Ltd., Diamond House, Harwell Science and Innovation Campus, Didcot, Oxfordshire OX11 0DE, United Kingdom*

(Received 13 November 2013; revised manuscript received 26 August 2014; published 6 October 2014)

The position of the band edges of a material plays a key role in determining the properties for a range of applications, but fundamental band bending is an interface-dependent property that cannot be quantified without knowledge of bulk electron energy levels. We present a method for calculating the bulk position of the valence band maximum, and therefore the *bulk* ionization potential, from periodic plane wave calculations as shown for a range of rocksalt ionic oxides. We demonstrate that, for the popular “slab alignment” technique, explicit consideration of any surface induced electronic polarization is necessary to calculate accurate bulk ionization potentials. Our proposed method to quantify these surface effects, using polarizable-shell based interatomic potentials, is very computationally affordable, and our updated slab alignment method yields much improved agreement with the available experimental data.

DOI: [10.1103/PhysRevB.90.155106](https://doi.org/10.1103/PhysRevB.90.155106)

PACS number(s): 71.15.Dx, 31.15.A–, 71.15.Mb, 71.20.–b

I. INTRODUCTION

Knowledge of ionization potentials, fundamental band bending, and electronic band alignment is crucial to our understanding of wide-ranging physical phenomena and chemical processes at the surfaces and interfaces of different materials [1]. A number of heterojunction alignment schemes have been advanced based on surface spectroscopic, electrical contact, or electrochemical measurements [1–7], which were also supported by electronic structure calculations, typically using density functional theory (DFT) [7–12]. Based on such schemes, complemented by studies of defect energetics, a concept of a fundamental charge neutrality level has been proposed that is common in all materials and exploited to interpret or predict defect properties and/or response to radiation [13–15]. The schemes, however, differ significantly in their positioning of the charge neutrality level with respect to vacuum or mutual band alignment. In contrast, the vacuum level itself is common to all materials by definition; it can serve as a common source or sink of charge for all finite samples. Therefore, establishing a robust and reliable methodology that will let us access this level from commonly employed *ab initio* techniques is necessary.

Currently, there are several computational approaches to the calculation of bulk ionization potentials and band alignment; each, however, has inherent difficulties. Indeed, we aspire to quantify a local property of the bulk system that is assumed to be independent of surface termination, and therefore periodic boundary conditions (PBC) are applied [16] to a unit cell for calculation purposes, most commonly in the context of Kohn-Sham equations [17,18], where the energy reference is a result of particular implementation of lattice sums [19] and, usually, is not trivial to assess. In one approach, physical models of real interfaces are constructed, thus providing directly the band structure across the interface [10,20–23]. Upon

formation of the interface between two different materials, a dipole is necessarily formed, which results in an offset in the electrostatic potential, for which in practice it is difficult to obtain a converged value [14]. An alternative method, which is less commonly applied, employs two-dimensional periodic slab models and provides direct access to a common reference level as an asymptote in vacuum, e.g., as implemented in CRYSTAL [24]. Here, the problem arises in turn from a dipole formed on surface termination, but at least now it depends on the properties of one material only, and the potential offset is the real physical origin of surface band bending. However, the two-dimensional (2D) lattice sums are not well suited for plane-wave methods, implemented in such popular codes as CPMD [25], CASTEP [26], and VASP [27,28]. To access the vacuum level from plane-wave calculations, a periodic slab model is commonly employed, akin to the 2D slab discussed above; however, a large interslab vacuum layer is created. The middle of the slab approximates the bulk, whereas the middle of the empty layer represents vacuum [29–34].

In this work, we demonstrate that, due to the lack of consideration for surface polarization, this approach results in errors even for the simplest rocksalt structured II-VI ionic oxides, themselves of scientific interest due to their applications as catalytic substrates [35,36] and characterizable electronic properties [37,38], some of which are quite unusual, e.g., negative electron affinity, or work function [39]. Furthermore, the stability of the (100) surfaces for these materials [40] means that experimental surface measurements can be compared to simulations without need for consideration of complex surface restructuring. We propose a scheme for calculating the position of the vacuum potential for bulk materials that takes advantage of the intuitive strengths of the previous method, but also takes into account the potential offset incurred through polarization effects, accounting for the electronic redistribution at the slab terminating surfaces in a semiclassical approximation. Our approach results in a substantial improvement in comparison to experiment, while being only slightly more computationally expensive.

*a.logsdail@ucl.ac.uk

†a.sokol@ucl.ac.uk

II. METHODOLOGY

A. Bulk ionization potential

By convention, the vacuum potential, V_{vac} , is the potential of an electron far removed from the bulk, and is set to zero. The difference between the highest occupied one-electron energy level of a system and the vacuum level, $-eV_{\text{vac}}$, is considered to be the first ionization potential of a system via Koopman's theorem [41]; while this approximation is not strictly valid for the Kohn-Sham formalism, the errors in the accuracy of resulting electronic energies have been shown to be small for bound states [42]. The highest occupied energy level (ϵ_{VBM}) is referred to as the energy of the valence band maximum (VBM) in bulk materials, and therefore the first ionization potential of the bulk can be defined as the energy required to move an electron from the VBM to vacuum [43]:

$$I_{\text{VBM}}^{\text{b}} = -eV_{\text{vac}} - \epsilon_{\text{VBM}}^{\text{b}} = -\epsilon_{\text{VBM}}^{\text{b}}, \quad (1)$$

where b denotes the bulk.

In gas-phase calculations, using for example localized basis sets, periodicity is not applied, and the concept of the vacuum potential far removed from a molecule is easily understood. However, the inherent periodicity of a plane-wave basis means that in periodic calculations one must create a vacuum region where V_{vac} can be accessed. Typically, this is achieved by creating a surface slab ‘‘supercell,’’ where a thick slab layer represents the bulk material, and a large interslab vacuum space is included to allow assessment of V_{vac} . In this case, however, the electrostatic potential does not disappear in the middle of the vacuum region (V_{bg}^{s} , where bg signifies the background level, and s signifies surface), but may remain finite [30,32] due to both the slow convergence of the 3D lattice sums with respect to the vacuum-layer width and/or the effects of surface band bending. However, V_{bg}^{s} is analogous to V_{vac} , and so the two may be aligned with a shift in energy equal in magnitude to $eV_{\text{bg}}^{\text{s}}$, with e being the electron charge. By shifting all the electron energies by the same quantity, the ‘‘absolute’’ electron energies for a slab can therefore be obtained [29,32], as illustrated in Fig. 1.

If the slab layer is thick enough then the atoms in the middle of the slab may be likened to being in a bulk environment; thus, it is possible to relate the energy levels for the central atoms of the slab to the energy levels of the same atoms in the bulk. Assuming that the lowest energy core states (e.g., 1s) on atoms in the middle of the slab are unperturbed by surface effects, due to their explicit localized nature, one can take such core states in the slab and calculate the difference between their energy (ϵ_c^{s} , where c signifies the core level) and the energy of the same quantum state in the bulk (ϵ_c^{b}) [44]:

$$\Delta\epsilon_c = \epsilon_c^{\text{b}} - \epsilon_c^{\text{s}}. \quad (2)$$

One can then define the ionization potential of the reference 1s core state in the slab model (I_c) as the energy required to take an electron from the core level (ϵ_c^{s}) to the midvacuum layer (V_{bg}^{s}); by convention this approximation then equates I_c to the ionization potential of the corresponding state in the bulk as [29]

$$I_c^{\text{s}} = -eV_{\text{bg}}^{\text{s}} - \epsilon_c^{\text{s}}, \quad (3)$$

$$I_c^{\text{b}} = -eV_{\text{bg}}^{\text{s}} - \epsilon_c^{\text{b}} + \Delta\epsilon_c = I_c^{\text{s}}, \quad (4)$$

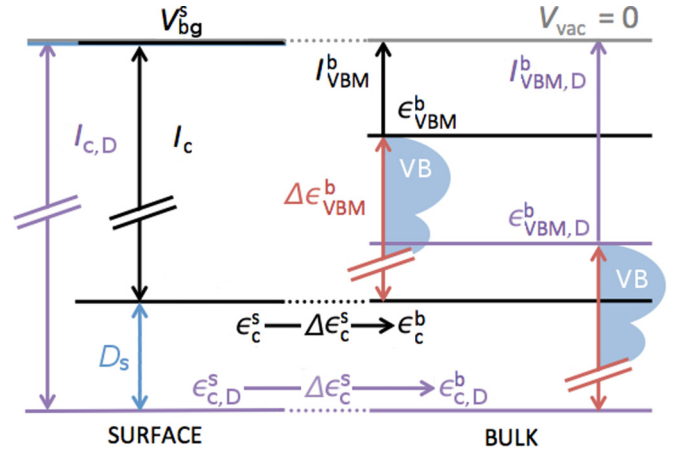


FIG. 1. (Color online) Diagram of vacuum alignment methods: I_c (black) is the difference between $-eV_{\text{bg}}^{\text{s}}$ and ϵ_c^{s} , and ϵ_c^{b} is the position of the core levels in bulk using this method; $I_{c,D}$ (purple) is the difference between $-eV_{\text{bg}}^{\text{s}}$ and ϵ_c^{s} with D_s considered explicitly, and $\epsilon_{c,D}^{\text{b}}$ is the position of the core levels in bulk using this method. $\Delta\epsilon_{\text{VBM}}^{\text{b}}$ (red) is the difference in energy between the core and valence levels in bulk, used to position the valence band maximum (VBM) by each method ($\epsilon_{\text{VBM}}^{\text{b}}$ and $\epsilon_{\text{VBM},D}^{\text{b}}$); VB (white) is the valence band; V_{vac} (gray) is the vacuum level. I_{VBM} is therefore the first ionization potential of the bulk, calculated as the difference between $-eV_{\text{vac}}$ and $\epsilon_{\text{VBM}}^{\text{b}}$ (black) and $\epsilon_{\text{VBM},D}^{\text{b}}$ (purple) and labeled as $I_{\text{VBM}}^{\text{b}}$ and $I_{\text{VBM},D}^{\text{b}}$, respectively.

and from this the states in the bulk system can be aligned to the vacuum level by shifting all the energy levels in the bulk by $\Delta\epsilon_c$. This therefore allows an *absolute* natural alignment of important bulk electron energies, such as ϵ_{VBM} , for different materials at the DFT level as the first ionization potential can now be defined as:

$$I_{\text{VBM}}^{\text{b}} = -eV_{\text{bg}}^{\text{s}} - \epsilon_{\text{VBM}}^{\text{b}} + \Delta\epsilon_c. \quad (5)$$

For a full understanding of surface properties, including surface band bending effects from different surfaces and/or interfaces, I_c^{b} provides a common reference energy. However, for a slab model with a fixed bulk geometry, introducing a surface will alter the electronic properties of a system: the additional electronic degrees of freedom will lead to electrons migrating to or away from the vacuum environment, resulting in the formation of surface multipoles that create an inherent offset in the electrostatic potential in a slab [45,46]. Therefore, we outline below a method that allows evaluation of surface polarization effects, which effectively recovers the surface independent nature of the alignment of bulk levels and thus offers the ability to calculate bulk ionization potentials; and only then can one begin to consider separately interface-dependent effects such as fundamental band bending. We note that the slab models could be geometry optimized for the calculation of surface specific properties, and then $\epsilon_{\text{VBM}}^{\text{s}}$ for a final geometry can be directly aligned with V_{bg}^{s} to give a valid *absolute* electron energy level for *this surface only*. The geometry optimized surfaces could also be used to assess bulk energy levels; however, the analysis is complicated by the additional optimization of nuclear coordinates, which may

lead to increases in surface polarization that can further shift ϵ_c^s [44]. Therefore, we emphasize here that the *simplest* method to assess ϵ_c^s accurately is by fixing the slab atomic structure to that of the bulk geometry.

In an ionic material, the shift in energy levels upon surface termination is correlated with changes in the underlying electrostatic potential; more specifically, electron redistribution will directly influence the electrostatic potential through the formation of surface multipoles. Therefore, changes in ϵ_c^s can be quantified by calculating the change in the electrostatic potential in the middle of the slab (ΔV_c^s) and in the middle of the vacuum gap (ΔV_{bg}^s) due to electron redistribution:

$$\Delta V_c^s = V_c^{s,relax} - V_c^s, \quad (6)$$

$$\Delta V_{bg}^s = V_{bg}^{s,relax} - V_{bg}^s, \quad (7)$$

where V_c^s and V_{bg}^s [as defined for Eq. (3)] are the electrostatic potentials *before* electron redistribution, and $V_c^{s,relax}$ and $V_{bg}^{s,relax}$ are the electrostatic potentials *after* electronic relaxation. With the nuclear coordinates fixed, an increase in ΔV_c^s indicates electron redistribution towards the surface, while a decrease results from electron redistribution towards the center of the slab. So in the absence of polarization, as in the bulk environment, $\Delta V_{bg}^s = \Delta V_c^s = 0$. We can therefore define the surface polarization correction as the multipolar shift, D_s :

$$D_s = e(\Delta V_{bg}^s - \Delta V_c^s), \quad (8)$$

where the dipolar parallel plate (planar) capacitor model is used to define the sign on ΔV_c^s and ΔV_{bg}^s : if an electronic dipole forms pointing in to the slab, with negative charge at the surface, then $\Delta V_c^s > 0 > \Delta V_{bg}^s$ [47]. This stabilizes ϵ_c^s relative to the V_{bg}^s , meaning that I_c^s would be inflated. To remove this dipolar effect, therefore, the polarization free environment must be recreated, as achieved by subtracting out the positive shift in electrostatic potential for the central atoms in the slab, $-e\Delta V_c^s$, and by adding $e\Delta V_{bg}^s$ to remove the negative shift in V_{bg}^s .

D_s can then be combined with I_c^b to provide an improved assessment of the bulk ionization potentials:

$$I_{c,D}^b = I_c^b + D_s, \quad (9)$$

where I_c^b is as defined in Eq. (4). Thus $I_{c,D}^b$ is the bulk ionization potential for the core levels *including* the effects for surface polarization, and bulk energy levels must be shifted by D_s , as well as $\Delta\epsilon_c$, in order to align them correctly with the V_{vac} . This applies to all energy levels and thus the first ionization potential, as defined in Eq. (5), similarly becomes $I_{VBM,D}^b = I_{VBM}^b + D_s$.

B. Computational details

DFT calculations have been performed using a plane-wave basis set, as implemented in the software package VASP [27,28], to obtain accurate electron energy levels. Only the valence electronic configurations were calculated explicitly, with interactions between the core and valence electrons described using the PAW method [48]. The valence electronic configurations for O ($2s^2 2p^4$), Mg ($2p^6 3s^2$), Ca ($3s^2 3p^6 4s^2$), Sr ($4s^2 4p^6 5s^2$), and Ba ($5s^2 5p^6 6s^2$) all included semicore states. A plane-wave kinetic energy cutoff of 500 eV and a con-

verged Monkhorst-Pack grid [49] across the first Brillouin zone with \mathbf{k} -points spacing of 0.04 \AA^{-1} or denser have been used throughout. The sole unit cell parameter for cubic rocksalts, a_0 , was optimized using the analytical stress tensor, and the plane waves were adjusted between geometry optimization steps to remove Pulay stress [50]. Structural convergence was achieved when the forces on all atoms were less than 0.01 eV \AA^{-1} . We have used the PBE [51] and PBESol [52] exchange-correlation (XC) functionals, which are both examples of the generalized gradient approximation (GGA), as well as their nonlocal hybrid counterparts, namely PBE0 [53] and PBESol0, wherein 25% of Hartree-Fock exchange is combined with the GGA XC functionals [53,54]. High-frequency dielectric constants were calculated via linear response density functional perturbation theory at all four levels of theory [55], with >200 unoccupied bands included in the calculation.

To represent surface termination, slab supercells were constructed from the optimized bulk unit cell with a (100) termination. The electronic structure in the middle of the slab should correctly reproduce the bulk electronic structure, and the slab is terminated with the (100) surface as this produces the lowest disturbance to the electronic structure, i.e. the fewest bonds are severed, has the lowest surface energy and, therefore, has the least effect on the electronic structure. Furthermore, a Tasker type 1 surface [56], with no residual polar moments, is preferably chosen; otherwise, higher order multipoles must be considered as contributing to D_s . A minimum of eight atomic layers in the slab model and a vacuum layer of at least 18 \AA proved necessary to converge the electronic properties in the middle of the slab, with ϵ_c^s converged to 0.01 eV . The electronic structure of the slab was then calculated with DFT, with the atomic structure fixed in the bulklike arrangement [29], and $-eV_{bg}^s$ is taken to be the Hartree potential (energy density) in the middle of the vacuum layer, as illustrated in Fig. 2.

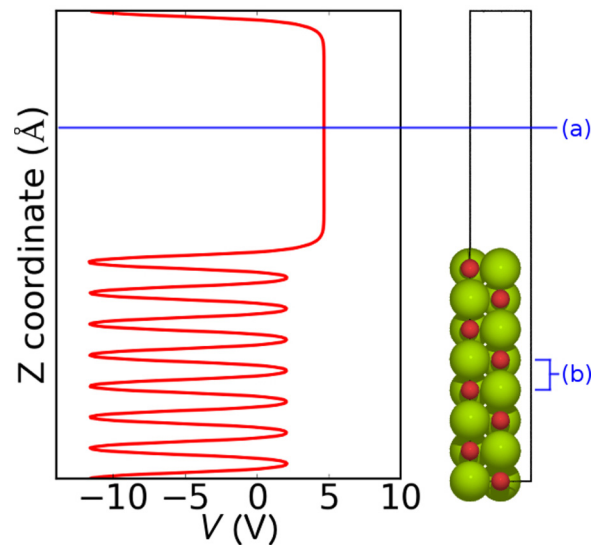


FIG. 2. (Color online) Example of an MgO surface unit cell (right) alongside a plot in red of the electrostatic potential normal to the slab surface, $V(z)$ (left). Highlighted in blue are (a) the midpoint of the interslab vacuum gap where V_{bg}^s is evaluated and (b) the middle atoms of the slab structure, on which both V_c^s and ϵ_c^s are evaluated. Mg and O atoms are shown in green and red, respectively.

To calculate ΔV_c^s and ΔV_{bg}^s , the effects of electronic relaxation in the supercell have been modeled as electronic polarization using the approach of Lewis and Catlow [57], in which an accurate account is given by the method of interatomic potentials coupled with a polarizable shell model as implemented in GULP [58]. In the polarizable shell model a harmonic energy contribution between the core and shell (U_{c-s}) for atom i is defined as

$$U_{c-s,i} = \frac{1}{2}k_i r_{c-s,i}^2, \quad (10)$$

where $r_{c-s,i}$ is the distance between the core and shell of i , and the spring constant k_i is defined as [58]

$$k_i = Y^2/\alpha_i, \quad (11)$$

where α_i is the polarizability, and Y is the shell charge of the respective ion. In this approach, cationic polarizabilities are assumed to be system independent and equal to those of gas phase ions (Lewis and Catlow have actually used the values of α_i originally tabulated by Pauling [59]), whereas the anionic polarizabilities are system and site dependent. The latter could be determined either by scaling the value of α_i taken from a system where such a value is known, using an approximate inverse proportionality of the polarizability and the Madelung site potential, or established empirically, for example by fitting the high-frequency dielectric constant or refractive indices. The potentials of Lewis and Catlow [57] were originally parametrized to experimentally observed properties, and we have reparametrized them to reproduce the bulk lattice (a_0) and high-frequency bulk dielectric [$\epsilon(\infty)$] constants as obtained from DFT calculations to a high degree of accuracy (0.0001%) for each XC functional. Furthermore, by taking into account that α_i is proportional to the site coordination number, we have reduced k_i by a coordination factor of n_b/n_i for each surface terminating site, where n_b and n_i are the coordination number for a bulk atom and atom i , respectively. The dependence of k_i on the atomic coordination therefore accounts for changes in polarizability at surfaces and interfaces.

Using the XC-specific parametrized potentials, the slab models were subjected to electronic minimization, in which the atomic cores were fixed and *only* the polarizable shells were allowed to move; thus representing the relaxation of valence electrons within the DFT slab calculation. ΔV_c^s and ΔV_{bg}^s were calculated as the differences in the Madelung site potentials before and after shell relaxation at the oxygen core and the mid-vacuum gap, respectively.

III. RESULTS AND DISCUSSION

Presented in Table I are first ionization potentials (negative of the positions of the VBM), as calculated from a full band structure, relative to vacuum for metal oxides formed by group 2 elements of the Periodic Table (MgO, CaO, SrO, and BaO) aligned using Eqs. (3), (4), and (9), as well as the industrially relevant group 12 metal oxide CdO. Details of shell model parametrization and results from our DFT and interatomic potential based calculations are provided in the Appendices. As we have shown for our slab model, electron energies converge within four atomic layers (~ 10 Å) and our calculated I_{VBM} can be compared directly to the experimental optical absorption spectra of mixed samples, where the

TABLE I. I_{VBM}^b and $I_{VBM,D}^b$ of rocksalt structured oxides, as calculated using Eqs. (3) and (9), respectively, to align the vacuum level. $I_{VBM,D}^b$ is presented in bold, while I_{VBM}^b is presented in italics. The bulk VBM were taken from Γ for MgO, CaO, and SrO, M for BaO, and L for CdO, respectively. For comparison, the first ionization potential as calculated from experimental optical absorption measurements is also presented where available [39,61–63], as well as an experimentally derived estimate for CdO from the work function [64–66].

	Expt.	PBE	PBESol	PBE0	PBESol0
MgO	7.16	5.75 (4.79)	5.81 (4.83)	6.89 (6.04)	6.97 (6.11)
CaO	6.25	4.67 (4.29)	4.74 (4.35)	5.64 (5.47)	5.90 (5.73)
SrO	5.30	4.22 (4.06)	4.31 (4.16)	5.21 (5.27)	5.30 (5.38)
BaO		3.37 (3.67)	3.32 (3.66)	4.14 (4.75)	4.17 (4.80)
CdO	6.04–6.78			6.35 (5.69)	5.94 (5.28)

penetration depth of incident radiation is several orders of magnitude greater than the depth of any possible surface band bending (e.g., ~ 25 μm for MgO [60]), and the (100) surfaces of these rocksalt structured materials are extremely stable with respect to other surfaces. Furthermore, surface rumpling on the (100) surface alters nuclear coordinates by at most 2% [40], and so it can be safely assumed that experimental optical measurements effectively evaluate I_{VBM}^b .

For all the XC functionals and materials considered, we observe changes in the *absolute* positioning of the VBM relative to V_{vac} for the different methods of vacuum alignment. Turning first to the GGA XC functionals, for PBE and PBESol the I_{VBM}^b (i.e., uncorrected for surface polarization) are significant underestimates of ca. 2 eV for MgO and CaO when compared to I_{expt} , and I_{VBM}^b of SrO is underestimated by ca. 1 eV. A better agreement is universally achieved for $I_{VBM,D}^b$ (i.e., corrected for surface polarization), with the multipolar shift D_s increase/decrease of up to 0.98/0.34 eV in the case of MgO/BaO, respectively. We also note that, when comparing XC functionals and alignment methods, PBESol provides a greater I_{VBM}^b for the rock salt oxides formed from lighter cations (Mg, Ca, Sr), while PBE gives a marginally greater I_{VBM}^b for the heavier Ba cation. All GGA calculations, however, significantly underestimate I_{VBM} compared to experiment—a well known artifact of the inability of GGA to exclude electron self-interaction with sufficient accuracy [67,68].

The use of nonlocal XC functionals has been shown to be an effective method to counteract the inadequacies of GGA functionals in representing electronic structure of ionic materials [54]. Unsurprisingly, the PBE0 results are qualitatively better than calculated for PBE, with underestimates for I_{VBM}^b compared to experiment of 0.63 and 0.75 eV for MgO and CaO, respectively, while the I_{VBM}^b of SrO is close to I_{expt} . We also calculated the I_{VBM}^b for CdO as 5.69 eV in this case, which is lower than our experimental estimates of 6.04–6.78 eV. This experimental estimate for CdO is obtained by combining band gap measurements (0.84 eV) with the electron affinity, which range over 5.2–5.94 eV [64–66]. Again, the results are

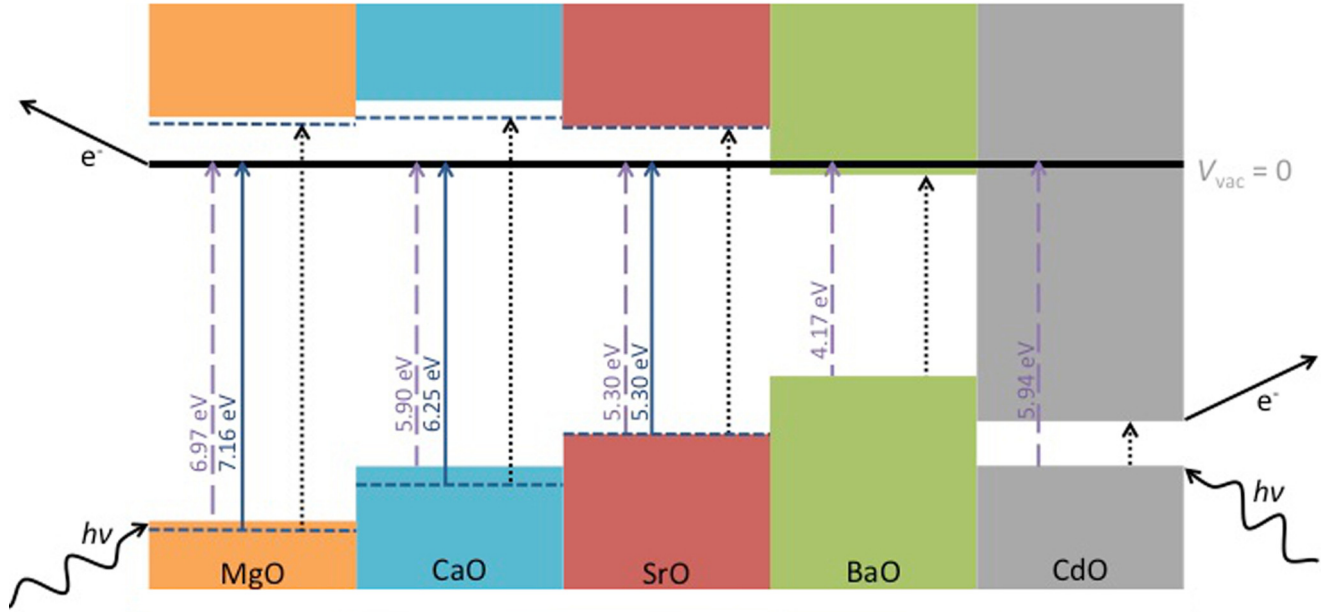


FIG. 3. (Color online) Schematic illustration of the ionization potential $I_{VBM,D}^b$ for MgO (orange), CaO (blue), SrO (pink), BaO (green), and CdO (gray), as calculated using the PBESol0 XC functionals. Vacuum alignments were calculated using $I_{c,D}$ in Eq. (9) and illustrated with purple dashed lines. Experimental first ionization potentials (I_{expt}) are also illustrated with blue arrows, and dashed blue horizontal markers. Black dotted lines mark out the experimental band gaps [64,69] and thus the position of the conduction band minimum relative to the vacuum is also illustrated. Experimental band gaps are chosen due to the uncertainty in the position of unoccupied orbitals at the DFT level, with calculated band gaps compared in the Appendices.

universally improved for $I_{VBM,D}^b$: the $I_{VBM,D}^b$ of MgO and CaO are now only underestimated by 0.27 and 0.58 eV, respectively, and the $I_{VBM,D}^b$ of SrO remains relatively constant with a difference of only 0.09 eV compared to I_{expt} . Furthermore, the $I_{VBM,D}^b$ of CdO is increased by 0.66 eV, to 6.35 eV, much closer to our experimental estimate.

Finally, we repeated all our calculations using the PBESol0 XC functional due to its success in reproducing bulk properties [70]. The resulting ionization potentials are all greater than those calculated using PBE0, in contrast to our observations for the GGA level of theory: the calculated $I_{VBM,D}^b$ of 6.97, 5.90, and 5.30 eV for MgO, CaO, and SrO deviate from experiment by only 0.19, 0.35, and 0.00 eV, respectively, as illustrated in Fig. 3. Special attention must be paid, however, to the position of the VBM of CdO in this case. When the vacuum level is aligned for PBESol0 using I_c [Eq. (3)], the VBM of CdO is positioned *above* both CaO and SrO. In contrast, when using PBE0, this same method positions the VBM for CdO *below* the VBM of CaO and SrO (Fig. 3). Thus an obvious question exists: which alignment is correct? $I_{c,D}$ [Eq. (9)] gives a more consistent answer, as for *both* nonlocal XC functionals the VBM of CdO is positioned *below* that of CaO and SrO.

Presented in Table II are ΔV_{bg}^s , ΔV_c^s , and D_s , as calculated using the reparametrized shell model potentials, for local (PBESol) and nonlocal (PBESol0) XC functionals. The similarity of calculated values between both types of XC functional is evident. Furthermore, the trend in results can be convincingly linked to the increasing cation radius as one descends the group: 0.86 Å (Mg), 1.14 Å (Ca), 1.32 Å (Sr), 1.49 Å (Ba), and the polarizability of the ionic oxides (results included in the Appendices). We note that the overall sign of

D_s correlates with the radius of the cation relative to the O anion, which has an ionic radius of 1.26 Å [71].

For the smaller Mg and Ca cations, the total shift in electrostatic potential is large and negative, implying that electrons distribute inward from the slab surface. This results in an underestimate of the ionization potential. For the Sr and Ba cations, which are larger than O anions, the shift in D_s is positive, highlighting electron accumulation towards the surface, though further verification is needed to study these effects for actual relaxed surfaces.

We note that the differences in the Madelung potential between equivalent sites in the bulk unit cell and the bulklike positions in the middle of the fixed slab supercell were used to give an accurate representation of the error bars in using the described “slab alignment” method. For the group 2 (12) metal oxides, the error bars are less than ± 0.02 (± 0.14) V before shell optimization.

TABLE II. Calculated shifts ΔV_{bg}^s and ΔV_c^s , respectively, in V, as a function of compound for the slab geometries as a result of shell relaxation. Results for the PBESol (*PBESol0*) XC functionals are presented. The combined polarization offset, D_s , is given in eV.

	MgO	CaO	SrO	BaO	CdO
ΔV_{bg}^s	0.45 (0.40)	0.21 (0.10)	0.10 (-0.02)	-0.14 (-0.29)	(0.51)
ΔV_c^s	-0.53 (-0.46)	-0.18 (-0.07)	-0.05 (0.06)	0.20 (0.34)	(-0.15)
D_s	0.98 (0.86)	0.39 (0.16)	0.16 (-0.08)	-0.34 (-0.63)	(0.66)

IV. CONCLUSIONS

In conclusion, we have investigated the slab model technique for vacuum alignment of energy levels in bulk materials at the plane-wave DFT level, and illustrated deficiencies in the application of this method. Explicit consideration of the electronic polarization, induced by the presence of a surface, is necessary for accurate results. We have proposed a method for quantifying the electronic polarization using simple polarizable shell-based interatomic potentials that have been tuned to reproduce accurately the properties predicted by DFT calculations. Our updated results for rocksalt ionic oxides using nonlocal XC functionals show excellent agreement with the available experimental literature when using our suggested bulk alignment protocol, illustrating the potential of this method. Our observations open a path to understanding the extent of fundamental band bending: knowledge of the bulk ionization potential would allow for the crystal engineering of band alignments for specific applications using band bending effects. Further work is ongoing to generalize our observations for more complex materials, as well as consideration of surfaces with intrinsic polar moments such as the more complex polymorphs of common semiconducting oxides.

ACKNOWLEDGMENTS

The authors acknowledge stimulating discussions with Aron Walsh and Keith Butler. A.J.L., C.R.A.C., and A.A.S. acknowledge funding from EPSRC Grants No. EP/IO30662/1 and No. EP/K038419/1. The authors acknowledge the use of the following high-performance computing facilities, and associated support services, in the completion of this work: HECToR, via our membership of the UK HPC Materials Chemistry Consortium (EP/L000202), IRIDIS, provided by the Centre for Innovation, and UCL Legion.

APPENDIX A: DFT OBSERVABLES: LATTICE PARAMETER, BAND GAP, AND POLARIZABILITY

The calculated DFT observables, as used to reparameterize the interatomic potentials and calculate the position of the valence band maximum, are presented. Namely, the data presented are the lattice parameter of the structure (Table III), the electronic band gap (Table IV), and the high-frequency dielectric constant (Table V).

TABLE III. DFT-calculated lattice parameter, a_0 (Å), for the cubic unit cells of MgO, CaO, SrO, BaO, and CdO, as optimized using the analytical stress tensor. Calculations were performed using the PBE, PBESol, PBE0, and PBESol0 exchange-correlation functionals, respectively. For comparison, experimental measurements from the literature at the lowest temperature available are also presented, with the temperature (K) given in parentheses [72–75].

	Expt.	PBE	PBESol	PBE0	PBESol0
MgO	4.21 (19.8)	4.26	4.22	4.21	4.18
CaO	4.80 (17.9)	4.84	4.78	4.80	4.77
SrO	5.16 (293)	5.19	5.14	5.17	5.12
BaO	5.54 (298)	5.61	5.53	5.56	5.52
CdO	4.70 (294)			4.72	4.67

TABLE IV. DFT-calculated band gap, E_g (eV), for the optimized cubic unit cells of MgO (Γ - Γ), CaO (Γ - M), SrO (Γ - M), BaO (M - M), and CdO (X - Γ). Calculations were performed using the PBE, PBESol, PBE0, and PBESol0 exchange-correlation functionals, respectively. For comparison, direct experimental measurements from the literature at the lowest temperature available are also presented (indirect for CdO; direct for all other materials), with the temperature (K) given in parentheses [64,69,76].

	Expt.	PBE	PBESol	PBE0	PBESol0
MgO	7.83 (85)	4.45	4.61	7.24	7.38
CaO	7.09 (85)	3.63	3.52	6.04	5.94
SrO	5.90 (55)	3.27	3.75	5.47	5.37
BaO	3.89 (55)	3.27	3.29	4.01	3.84
CdO	0.85 (100)			1.56	1.55

TABLE V. DFT-calculated high-frequency dielectric constant, $\epsilon(\infty)$, for the optimized cubic unit cells of MgO, CaO, SrO, BaO, and CdO. Calculations were performed using the PBE, PBESol, PBE0, and PBESol0 exchange-correlation functionals, respectively. For comparison, experimental measurements from the literature are also presented [77–80].

	Expt.	PBE	PBESol	PBE0	PBESol0
MgO	2.96	3.26	3.33	2.61	2.63
CaO	3.33	3.91	4.01	2.99	3.03
SrO	3.46	3.95	4.07	3.03	3.09
BaO	3.90	4.46	4.62	3.31	3.38
CdO	5.3			4.01	4.05

TABLE VI. Parameters for optimized interatomic potentials of MgO, CaO, SrO, BaO, and CdO, respectively. The interaction parameter, A (eV), between the cation and anion shells in each system, and the anion shell spring constant, k ($\text{eV}\text{\AA}^{-2}$), have been tuned to reproduce a_0 and $\epsilon(\infty)$ from DFT calculations, as performed using the PBE, PBESol, PBE0, and PBESol0 exchange-correlation functionals, respectively. All other components of the interatomic potentials were unaltered from the original work of Lewis and Catlow [57]. For the CdO system, the Cd^{2+} cation was modeled as an unpolarizable species, due to the absence in the literature of a completely polarizable potential for this system. In all cases the observables calculated using the tuned interatomic potential were within 0.0001% of the same DFT observables after fitting.

		PBE	PBESol	PBE0	PBESol0
MgO	$A(\text{Mg-O})$	1517.21	1447.76	1431.20	1383.76
	$k(\text{O})$	47.59	48.08	66.39	66.99
CaO	$A(\text{Ca-O})$	1124.32	1061.06	1085.33	1042.17
	$k(\text{O})$	37.08	37.97	58.98	60.30
SrO	$A(\text{Sr-O})$	996.37	944.34	969.30	921.57
	$k(\text{O})$	34.68	35.33	58.97	60.37
BaO	$A(\text{Ba-O})$	984.53	917.18	941.69	907.33
	$k(\text{O})$	30.76	32.06	55.06	55.83
CdO	$A(\text{Cd-O})$			870.82	827.33
	$k(\text{O})$			29.9196	30.4693

APPENDIX B: FORCEFIELD PARAMETERS: SHELL MODEL

The optimized interatomic potentials, as used in the calculation of the surface polarization effects, are presented

in Table VI for the rocksalt structured systems of interest: MgO, CaO, SrO, BaO and CdO.

-
- [1] A. Franciosi and C. G. V. de Walle, *Surf. Sci. Rep.* **25**, 1 (1996).
- [2] S. F. J. Cox, J. L. Gavartin, J. S. Lord, S. P. Cottrell, J. M. Gil, H. V. Alberto, J. P. Duarte, R. C. Vilão, N. A. de Campos, D. J. Keeble, E. A. Davis, M. Charlton, and D. P. van der Werf, *J. Phys.: Condens. Matter* **18**, 1079 (2006).
- [3] W. R. Frensley and H. Kroemer, *J. Vac. Sci. Technol.* **13**, 810 (1976).
- [4] W. R. Frensley and H. Kroemer, *Phys. Rev. B* **16**, 2642 (1977).
- [5] W. A. Harrison, *J. Vac. Sci. Technol.* **14**, 1016 (1977).
- [6] W. A. Harrison, *J. Vac. Sci. Technol. B* **3**, 1231 (1985).
- [7] D. O. Scanlon, C. W. Dunnill, J. Buckeridge, S. A. Shevlin, A. J. Logsdail, S. M. Woodley, C. R. A. Catlow, M. J. Powell, R. G. Palgrave, I. P. Parkin, G. W. Watson, T. W. Keal, P. Sherwood, A. Walsh, and A. A. Sokol, *Nat. Mater.* **12**, 798 (2013).
- [8] C. G. Van de Walle and R. M. Martin, in *Electronic Structure of Semiconductor Heterojunctions*, edited by G. Margaritondo, Perspectives in Condensed Matter Physics Vol. 1 (Springer, Netherlands, 1988), pp. 268–279.
- [9] C. G. Van de Walle and J. Neugebauer, *Nature (London)* **423**, 626 (2003).
- [10] Y.-H. Li, A. Walsh, S. Chen, W.-J. Yin, J.-H. Yang, J. Li, J. L. Da Silva, X. Gong, and S.-H. Wei, *Appl. Phys. Lett.* **94**, 212109 (2009).
- [11] S. B. Zhang, S.-H. Wei, and A. Zunger, *Phys. Rev. Lett.* **84**, 1232 (2000).
- [12] C. Kilic and A. Zunger, *Appl. Phys. Lett.* **81**, 73 (2002).
- [13] J. Tersoff, *Phys. Rev. B* **30**, 4874 (1984).
- [14] F. Flores and C. Tejedor, *J. Phys. C: Solid State* **12**, 731 (1979).
- [15] W. Mönch, *J. Appl. Phys.* **109**, 113724 (2011).
- [16] F. Jensen, *Introduction to Computational Chemistry* (Wiley, Chichester, 1999).
- [17] P. Hohenberg and W. Kohn, *Phys. Rev.* **136**, B864 (1964).
- [18] W. Kohn and L. J. Sham, *Phys. Rev.* **140**, A1133 (1965).
- [19] P. P. Ewald, *Ann. Phys.* **369**, 253 (1921).
- [20] A. Baldereschi, S. Baroni, and R. Resta, *Phys. Rev. Lett.* **61**, 734 (1988).
- [21] Y. Z. Zhu, G. D. Chen, H. Ye, A. Walsh, C. Y. Moon, and S.-H. Wei, *Phys. Rev. B* **77**, 245209 (2008).
- [22] A. Janotti and C. G. Van de Walle, *Phys. Rev. B* **75**, 121201 (2007).
- [23] S.-H. Wei and A. Zunger, *Appl. Phys. Lett.* **72**, 2011 (1998).
- [24] R. Dovesi, R. Orlando, B. Civalleri, C. Roetti, V. R. Saunders, and C. M. Zicovich-Wilson, *Z. Kristallogr.* **220**, 571 (2005).
- [25] R. Car and M. Parrinello, *Phys. Rev. Lett.* **55**, 2471 (1985).
- [26] M. D. Segall, P. J. D. Lindan, M. J. Probert, C. J. Pickard, P. J. Hasnip, S. J. Clark, and M. C. Payne, *J. Phys.: Condens. Matter* **14**, 2717 (2002).
- [27] G. Kresse and J. Furthmüller, *Comput. Mater. Sci.* **6**, 15 (1996).
- [28] G. Kresse and D. Joubert, *Phys. Rev. B* **59**, 1758 (1999).
- [29] B. Höfiling, A. Schleife, F. Fuchs, C. Rödl, and F. Bechstedt, *Appl. Phys. Lett.* **97**, 032116 (2010).
- [30] M. C. Toroker, D. K. Kanan, N. Alidoust, L. Y. Isseroff, P. Liao, and E. A. Carter, *Phys. Chem. Chem. Phys.* **13**, 16644 (2011).
- [31] D. West, Y. Y. Sun, and S. B. Zhang, *Appl. Phys. Lett.* **101**, 082105 (2012).
- [32] B. Höfiling, A. Schleife, C. Rödl, and F. Bechstedt, *Phys. Rev. B* **85**, 035305 (2012).
- [33] L. A. Burton and A. Walsh, *Appl. Phys. Lett.* **102**, 132111 (2013).
- [34] A. Walsh and C. R. A. Catlow, *J. Mater. Chem.* **20**, 10438 (2010).
- [35] J. Carrasco, F. Illas, and N. Lopez, *Phys. Rev. Lett.* **100**, 016101 (2008).
- [36] L. B. Vilhelmsen and B. Hammer, *Phys. Rev. Lett.* **108**, 126101 (2012).
- [37] N. A. Richter, S. Siculo, S. V. Levchenko, J. Sauer, and M. Scheffler, *Phys. Rev. Lett.* **111**, 045502 (2013).
- [38] P. Rinke, A. Schleife, E. Kioupakis, A. Janotti, C. Rödl, F. Bechstedt, M. Scheffler, and C. G. Van de Walle, *Phys. Rev. Lett.* **108**, 126404 (2012).
- [39] B. Ulrici, W. Ulrici, and N. N. Kovalev, *Fiz. Tverd. Tela* **17**, 3533 (1975) [*Sov. Phys. Solid State* **17**, 2305 (1975)].
- [40] P. Broqvist, H. Grönbeck, and I. Panas, *Surf. Sci.* **554**, 262 (2004).
- [41] T. Koopmans, *Physica* **1**, 104 (1934).
- [42] E. J. Baerends, O. V. Gritsenko, and R. van Meer, *Phys. Chem. Chem. Phys.* **15**, 16408 (2013).
- [43] A. Walsh and K. T. Butler, *Acc. Chem. Res.* **47**, 364 (2014).
- [44] K. T. Butler, J. Buckeridge, C. R. A. Catlow, and A. Walsh, *Phys. Rev. B* **89**, 115320 (2014).
- [45] Z. Zhang and J. T. Yates, *Chem. Rev.* **112**, 5520 (2012).
- [46] K. T. Butler and A. Walsh, *Thin Solid Films* **559**, 64 (2014).
- [47] L. Guimarães, H. A. de Abreu, and H. A. Duarte, *Chem. Phys.* **333**, 10 (2007).
- [48] P. E. Blöchl, *Phys. Rev. B* **50**, 17953 (1994).
- [49] H. J. Monkhorst and J. D. Pack, *Phys. Rev. B* **13**, 5188 (1976).
- [50] G. P. Francis and M. C. Payne, *J. Phys.: Condens. Matter* **2**, 4395 (1990).
- [51] J. P. Perdew, K. Burke, and M. Ernzerhof, *Phys. Rev. Lett.* **77**, 3865 (1996).
- [52] J. P. Perdew, A. Ruzsinszky, G. I. Csonka, O. A. Vydrov, G. E. Scuseria, L. A. Constantin, X. Zhou, and K. Burke, *Phys. Rev. Lett.* **100**, 136406 (2008).
- [53] C. Adamo and V. Barone, *J. Chem. Phys.* **110**, 6158 (1999).
- [54] M. Marsman, J. Paier, A. Stroppa, and G. Kresse, *J. Phys.: Condens. Matter* **20**, 064201 (2008).
- [55] M. Gajdoš, K. Hummer, G. Kresse, J. Furthmüller, and F. Bechstedt, *Phys. Rev. B* **73**, 045112 (2006).
- [56] P. W. Tasker, *J. Phys. C: Solid State* **12**, 4977 (1979).
- [57] G. V. Lewis and C. R. A. Catlow, *J. Phys. C: Solid State* **18**, 1149 (1985).
- [58] J. D. Gale and A. L. Rohl, *Mol. Simul.* **29**, 291 (2003).

- [59] L. Pauling, *Proc. R. Soc. A* **114**, 181 (1927).
- [60] E. D. Palik, *Handbook of Optical Constants of Solids* (Academic Press, New York, 1985).
- [61] P. D. Johnson, *Phys. Rev.* **94**, 845 (1954).
- [62] V. I. Neeley and J. C. Kemp, *J. Phys. Chem. Solids* **24**, 1301 (1963).
- [63] T. Jaouen, G. Jézéquel, G. Delhaye, B. Lépine, P. Turban, and P. Schieffer, *Appl. Phys. Lett.* **97**, 232104 (2010).
- [64] F. P. Koffyberg, *Phys. Rev. B* **13**, 4470 (1976).
- [65] W.-M. Cho, G.-R. He, T.-H. Su, and Y.-J. Lin, *Appl. Surf. Sci.* **258**, 4632 (2012).
- [66] D. Speaks, M. Mayer, K. Yu, S. Mao, E. Haller, and W. Walukiewicz, *J. Appl. Phys.* **107**, 113706 (2010).
- [67] J. P. Perdew and M. Levy, *Phys. Rev. Lett.* **51**, 1884 (1983).
- [68] L. J. Sham and M. Schlüter, *Phys. Rev. Lett.* **51**, 1888 (1983).
- [69] A. S. Rao and R. J. Kearney, *Physica Status Solidi (b)* **95**, 243 (1979).
- [70] *Chemical Modelling*, edited by M. Springborg, SPR–Chemical Modelling Vol. 9 (The Royal Society of Chemistry, Cambridge, UK, 2012), pp. P001–217.
- [71] R. D. Shannon, *Acta Crystallogr.* **32**, 751 (1976).
- [72] D. K. Smith and H. R. Leider, *J. Appl. Crystallogr.* **1**, 246 (1968).
- [73] J. Bashir, R. T. A. Khan, N. M. Butt, and G. Heger, *Powder Diffr.* **17**, 222 (2002).
- [74] R. J. Zollweg, *Phys. Rev.* **100**, 671 (1955).
- [75] A. Cimino and M. Marezio, *J. Phys. Chem. Solids* **17**, 57 (1960).
- [76] R. Whited, C. J. Flaten, and W. C. Walker, *Solid State Commun.* **13**, 1903 (1973).
- [77] R. E. Stephens and I. H. Malitson, *J. Res. Natl. Bur. Stand. (US)* **49**, 249 (1952).
- [78] J. Jacobson and E. Nixon, *J. Phys. Chem. Solids* **29**, 967 (1968).
- [79] C. J. Anderson and E. B. Hensley, *J. Appl. Phys.* **46**, 443 (1975).
- [80] H. Finkenrath, H. Köhler, and M. Lochmann, *Z. Ang. Phys.* **21**, 512 (1966).